



IMPACT OF VISCOUS DAMPING MODEL ASSUMPTIONS ON THE NONLINEAR ANALYSIS OF MULTI-SPAN BRIDGES

D.R. Martinez⁽¹⁾, M.J. Kowalsky⁽²⁾

⁽¹⁾ Ph.D. Candidate, North Carolina State University, drmarti6@ncsu.edu

⁽²⁾ Professor-Structural Engineering, North Carolina State University, kowalsky@ncsu.edu

Abstract

In the performance-based design of bridges (PBD), the accurate determination of deformation demands is essential to ensure that structures achieve their intended performance. An integral part of advanced PBD approaches are design verification techniques such as Nonlinear Time-History Analysis (NLTHA). One assumption that has proven essential but is not well understood by engineers is the impact that viscous damping might have on the nonlinear response of structures. Other researchers have shown that for Single-Degree-of-Freedom (SDOF) systems, the displacement time histories from shake table tests compare much better with a Stiffness-Proportional Damping Model using a Tangent Stiffness rather than an Initial Stiffness approach. Conversely, the problem is that the Initial Stiffness option is normally the damping method that is included in most computational platforms, and many engineers are not aware of the consequences that might have on the predictions of displacement response. In the case of Multi-Degree-of-Freedom (MDOF) bridges, little research has been done on this problem, and experimental verification is difficult due to the cost and complexity of tests at such a scale. Hence, in this study an extensive sensitivity analysis using NLTHA is performed for the transverse direction of three configurations of multi-span reinforced-concrete bridges, considering parameters such as the directivity of the ground motion, abutment restraint, and a concentrated-plasticity model in Ruaumoko3D. Seven damping models, such as the Modal Damping, Rayleigh (Mass and Stiffness terms), Stiffness-Proportional (Initial and Tangent) and Zero Viscous Damping, were considered. The results show that Modal Damping leads to the minimum seismic demands in all the models, while the Tangent Stiffness-Proportional model and Zero Viscous Damping lead to the largest displacements. The range of difference in the transverse displacements between the Modal Damping (lower limit) and the Zero Viscous Damping (upper limit) is from 32% to 72% for bridges with free abutments. In contrast, a difference from 42% to 69% was seen for structures with pinned abutments. Finally, the impact of the selection of a viscous damping model on the response of an existing bridge is presented. The Anchorage Port Access Bridge (Alaska) is a 700-meter long steel bridge that was analyzed using several damping models. Its hysteretic response was calibrated from two quasi-static tests on half-scale models conducted at the Constructed Facilities Lab at NC State. A difference in some piers of more than 100% among the damping models was observed when the bridge was subjected to the 2018 Anchorage earthquake that was spectrally matched to the AASHTO design spectrum. Thus, the results of both analyses highlight the profound influence that the choice of the viscous damping model may have on the inelastic response of bridges.

Keywords: Performance-Based Design, NLTH Analysis, Viscous Damping, Damping Models, Port Access Bridge.



1. Introduction

The philosophy of Performance-Based Design (PBD) has gained popularity with engineers as it allows structures to be designed to achieve prescribed performance levels for defined seismic hazards. In this context, Non-linear Time History Analysis (NLTHA) is the most sophisticated method currently available for design verification. In inelastic analyses, Rayleigh damping is the viscous damping model that is preferred by practitioners as it uses a combination of the Mass and Stiffness matrices to construct the damping matrix. However, researchers have found problems with Rayleigh damping models for nonlinear analysis of Multi-degree of Freedom Structures (MDOF).

Many researchers have studied this phenomenon. Crisp [1] and then Bernal [2] were the first to identify the high damping forces that can be produced in an inelastic analysis that uses initial proportional Rayleigh damping. Similarly, Leger et al. [3] studied the effects of various viscous damping models (Rayleigh, mass-proportional and stiffness-proportional damping) on MDOF structures. They recommended a range of periods for the structure where it is suitable to use either the initial or the tangent stiffness. Priestley & Grant [4] suggested using the tangent stiffness proportional damping (with special care in the selection of the damping associated with the first mode as the structure will act as if initial stiffness proportional damping has been prescribed, even if tangent stiffness is specified in the analysis). Consequently, Kowalsky & Hasgul [5] studied the impact of initial and tangent stiffness proportional damping on SDOF systems using various hysteretic rules obtaining a significant difference between both models. On the other hand, Hall [6] stated that the mass proportional term of the Rayleigh approach cannot possibly exist for analysis with dynamic loads and proposed to limit the high damping forces by capping the stiffness-proportional factor, eliminating the mass-proportional damping contribution. In response, Charney [7] recommended to eliminate the use of viscous damping and to rely only upon hysteretic damping for nonlinear analysis. More recently, Hall [8] performed an analysis studying the influence of different damping models on the inelastic response of moment-frame buildings. He stated that initial proportional damping should not be used for inelastic seismic analysis.

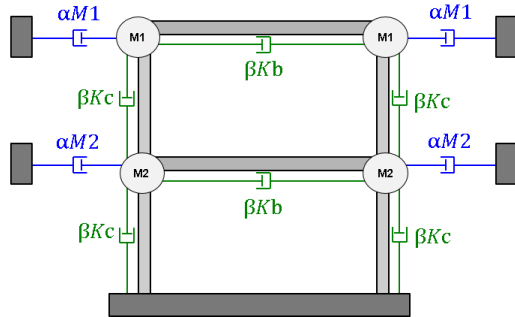
Other investigators such as Chopra & McKenna [9] and Carr [10] [11] have recommended using the superposition of modal damping matrices (Wilson-Penzien) for nonlinear analysis of buildings since this approach completely eliminates the spurious damping forces when the structure yields. Nonetheless, Petrini et al. [12] found that the analytical response of a concentrated plasticity model for a SDOF reinforced concrete column with tangent stiffness proportional damping was the closest to the results of a shaking table test. This was obtained through the comparison of concentrated and plasticity models (using initial and tangent stiffness proportional damping models) with the experiments. Despite this, Smyrou et al. [13] point out that for MDOF systems the stiffness proportional damping model overestimates the damping for higher modes. They suggested to model elastic damping in NLTHA for cantilever Reinforced Concrete (RC) walls using Modal Damping with an artificial lowering of the damping ratio in the first mode as proposed by Priestley and Grant [4]. In this case, the damping in the first mode will have similar behavior as the tangent stiffness proportional damping obtained by Petrini et al.

Based on the existing literature, there are many options to model viscous damping in NLTHA. Nevertheless, most of the recommendations are given for buildings, where non-structural components contribute to damping. In the cases of bridges, where the structural system approaches a “bare-frame”, research is limited. In the present paper, the aim is not to recommend the most appropriate damping model for nonlinear analysis of structures, since that conclusion only can be reached through experimental verification. Instead, we present the impact on the deformation demands for bridges due to the selection of various damping models for nonlinear analysis. This will be carried out through the study of viscous damping models based on both Rayleigh and Modal Damping. First, the results of NLTHA for these damping models will be evaluated for three four-span RC bridges. Then, the impact of viscous damping will be shown through the seismic assessment of the Anchorage Port Access Bridge, which is a 787-m long, irregular and highly complex steel bridge, situated in Anchorage, Alaska.

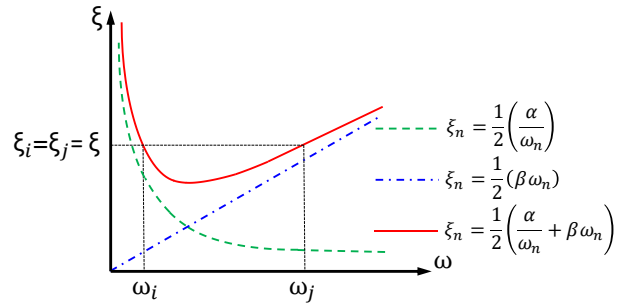


2. Damping Models

2.1 Rayleigh Damping



(a) Physical Meaning



(b) Mass and Stiffness Terms

Fig. 1 – Rayleigh Damping Model (adapted from [14]).

This damping model is commonly known as Proportional damping and is expressed as follows:

$$c = \alpha m + \beta k \quad (1)$$

Where the coefficients α and β are calculated by selecting two modes of vibration, m corresponds to the mass matrix of the structure, and k is the stiffness matrix. The meaning of Rayleigh damping is illustrated in Figure 1(a), where a 2-story frame with beam and column stiffness K_b and K_c , respectively, is shown. The coefficient βk simulates internal viscous dampers and acts in parallel with the elements. On the other hand, the term αm corresponds to viscous dampers that connect the masses M_1 and M_2 to external fixed points [14]. This model simulates the damping associated with the mass and stiffness of the structure and from Figure 1(b) is seen that for the lower frequencies, the damping ratio will be higher and will depend strongly on the mass coefficient term (dashed green line). In contrast, for the higher modes, the stiffness proportional term will dominate the calculation of the damping ratio. Special care has to be taken for higher modes, where the damping ratio grows linearly and there is low apportion of the mass term as in these cases a very high value of damping might be assigned to these upper modes.

This stiffness matrix (k) can be computed considering the initial or the current stiffness of the structure. This is known as the initial and tangent stiffness, respectively. The latter approach can be calculated using a tangent or a secant damping matrix. In the case of the tangent stiffness with the tangent damping matrix, the stiffness has hysteresis and the damping actions are not zero when the velocities are zero [11]. In contrast, the option of the tangent stiffness with the secant damping variation does not have those issues. Therefore, this is the recommended approach to model the tangent stiffness for NLTHA and the one considered in this paper.

2.2 Modal Damping

Wilson and Penzien (1972) showed that the damping matrix considering only the N mode shapes of free vibration will produce a Caughey damping model more easily. This procedure is based on the orthogonalization of the lateral mode shapes, resulting in a fully populated damping matrix obtained by summing individual matrices for each mode. This approach was not initially popular as it increased the processing time of the response history analysis due to the fully populated matrix. However, given the power of modern computers, it has recently gained popularity and is the method recommended by some academics to conduct nonlinear analysis [9] [11]. Equation 2 shows the representation of this approach.

$$c = \sum_{i=1}^n \frac{2 \cdot \xi_i \cdot \omega_i}{M_i} (m \cdot \phi_i) (\phi_i^T \cdot m) \quad (2)$$



In Equation 2, N corresponds to the number of damped modes, T_n is the mode period, ξ_n is the fraction of critical damping, m is the mass matrix, Φ_n is the mode shape, and ω_i is the circular natural frequency.

3. Numerical Study for Three Four-Span Bridges

The impact of viscous damping model assumptions will be assessed through evaluating the nonlinear response of three reinforced concrete bridges using various damping models. The structures selected represent typical geometric configurations from Alaska and were based on the work done by Kong [15]. The geometry of these bridges can be seen in Figure 5. The structures have four circular columns of different heights (8m, 12m, 14m, and 17m) but same diameter (2m). The materials of the structure have a concrete compression strength (f'_c) of 30 MPa and yield stress for the longitudinal and transverse steel of 420 MPa. The dead load from the superstructure is 120 kN/m, which produces an axial load ratio of 7% for the columns. A 1% of steel ratio was considered for the longitudinal and transverse steel reinforcing ratio of the columns. Also, the abutments were assumed to behave free or restricted to translate in the transverse direction, while for the longitudinal direction a bilinear elastic hysteresis loop with a GAP of 0.075m was considered. It is assumed that the superstructure is supported on elastomeric bearings, therefore the columns will behave in single bending in the transverse direction. The yield displacements using the approach proposed by Priestley et al. [16] for the columns of 8m, 12m, 14m, and 17m are 0.06m, 0.13m, 0.18m, and 0.26m, respectively. The Mander model [17] was used to calculate the confined properties of the sections and later was employed to obtain the moment-curvature relationship with an equivalent yield moment of 14160 kN*m. Using this, the cracked section moment of inertia was calculated to be 0.21m⁴ for the elements of the substructure. The nonlinear time-history analyses were performed using Ruaumoko3D [11], where a lumped plasticity model based on Giberson's one-component element was used for the modeling of the bridges. It was assumed that the inelasticity was concentrated only at the ends of the column, and the superstructure was modeled as elastic. Lastly, a bi-directional analysis using the two horizontal and perpendicular components of the ground motions was considered.

3.1 Demands

The analyses of the structures were carried out using a suite of unscaled ground motions from the Pacific Earthquake Engineering Research Center (PEER). Seven near-field pairs of ground motions were selected considering moment magnitudes (M_w) between 6.5 and 7.5 and epicentral distances less than 20 km. The main characteristics of these records are summarized in Table 1.

Table 1 – Characteristics of Ground Motions

Eq	Earthquake Name	Station Name	Magnitude	Mechanism	Rrup (km)	Vs30 (m/sec)
1	Loma Prieta	Gilroy Array #3	6.93	Reverse Oblique	12.82	349.85
2	Northridge-01	Canyon Country - W Lost Cany	6.69	Reverse	12.44	325.60
3	Duzce_Turkey	Bolu	7.14	Strike slip	12.04	293.57
4	El Mayor-Cucapah_Mexico	Michoacan de Campo	7.20	Strike slip	15.91	242.05
5	El Mayor-Cucapah_Mexico	Riito	7.20	Strike slip	13.71	242.05
6	El Mayor-Cucapah_Mexico	El Centro Array #11	7.20	Strike slip	16.21	196.25
7	Darfield_New Zealand	DFHS	7.00	Strike slip	11.86	344.02

The demands on the bridges were calculated using an AASHTO design response spectrum, which has a probability of exceedance of 7% in 75 years (approximately a return period of 1000 years). For this scenario, the bridges are situated in Anchorage, Alaska, and have a PGA of 0.538g, S_s of 1.183g, S_1 of 0.458g, and a soil site class D. Note that the records selected from the PEER have a shear velocity at a depth of 30 meters between 180 and 360 m/s, which make them compatible with the soil class D.

Figure 2(a) shows the acceleration response spectrum for the individual components of the seven pairs of earthquakes selected for the analysis, and they are contrasted with the AASHTO design spectrum for the



bridges. The AASHTO design spectrum is obtained using the geometric means, which is essentially the same as the RotD50 definition, which corresponds to the median of the response spectra of SDOF oscillators (See Boore et al. [18]). The RotD50 for the seven pairs of ground motions can be seen in Figure 2(b). These records were selected because their RotD50 representation was the best fit for the design spectra used in the analysis.

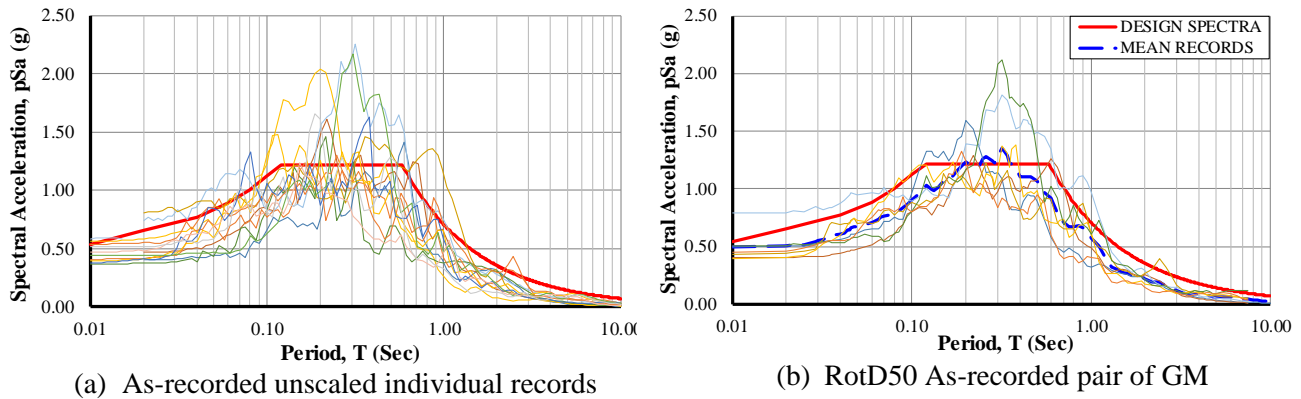


Fig. 2 – Acceleration Response Spectrum of Ground Motions Selected for Analysis.

The calculation of the demands for the bridges was performed using the as-recorded unscaled records described previously and the ground motions were then spectrally matched to the design spectrum for a range of periods between 0.10 sec and 5.00 sec, which corresponds to the interval of elastic and inelastic periods of the structures. This was done using the Matlab Code ArtifQuakeLetII [19] and is shown in Figure 3(a). Conversely, the RotD50 for the seven pairs of ground motions were spectrally matched to the design spectra and are shown in Figure 3(b). Note how the RotD50 response spectrum for each one of the records matches relatively well with the AASHTO spectrum.

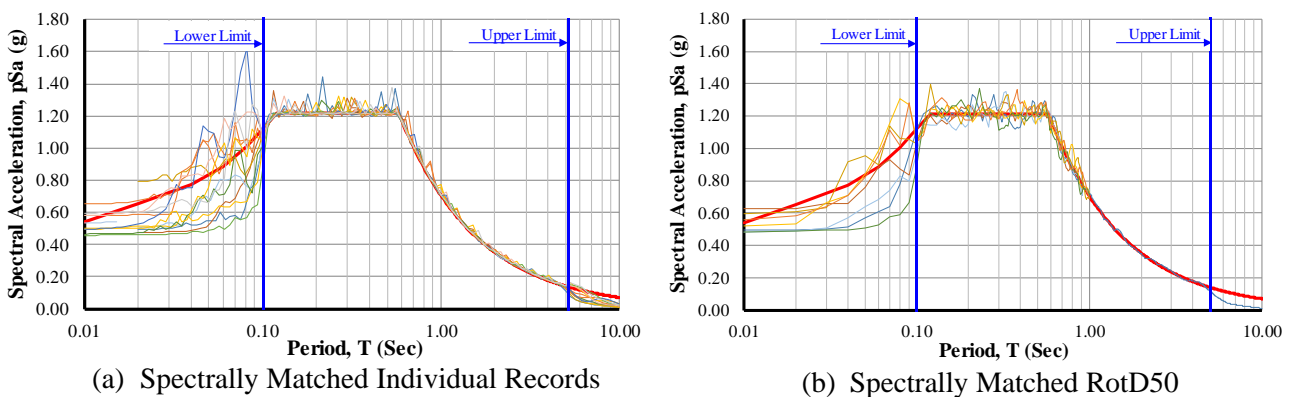


Fig. 3 – Acceleration Response Spectrum of Spectrally Matched Records.

3.2 Damping Models

Modal and Rayleigh Damping were selected to conduct the nonlinear analysis. In the case of Rayleigh damping, numerous variations were used to see its influence on the results. The seven types of damping models used in this paper are summarized in Table 2.

Table 2 shows that DM1 corresponds to Modal Damping, which has a viscous damping (ξ) value of 5% for all the modes of the structures. DM2 is calculated using a Rayleigh damping approach for modes 1 and 2 using Initial Stiffness. Generally, this model represents the most common damping model in practice. DM3 and DM4 are calculated using modes 1 and 10 for the initial and tangent stiffness with secant damping variation, respectively. The selection of mode 10 represents the upper limit at which 100 % of the mass will be achieved for all the structures (see Figure 4a). DM5 and DM6 correspond to the stiffness proportional damping models



using the initial and tangent stiffness, respectively. In both cases, the coefficient β was calculated using a 5% of viscous damping for modes 1 and 2 and eliminating the mass term. This produces that the first modes are underdamped, while the upper modes are not as overdamped as it would be the case assuming 5% for the first mode of the structures. Finally, DM7 represents the upper limit of the nonlinear response where zero viscous damping is considered. The distribution of viscous damping for the seven damping models used in this study are shown in Figure 4(b) for Bridge 1.

Table 2 – Characteristics of Damping Models used in the analysis.

DAMPING MODEL	NOMENCLATURE	TYPE OF DAMPING	Mode 1	ξ_1 %	Mode 2	ξ_2 %
DM1	MOD	Modal (Wilson-Penzien)	1	5	2	5
DM2	M+K0-1&2	Rayleigh M&K- Initial Stiffness	1	5	2	5
DM3	M+K0-1&10	Rayleigh M&K- Initial Stiffness	1	5	10	5
DM4	M+KS-1&10	Rayleigh M&K- Tangent Stiffness (Secant Variation)	1	5	10	5
DM5	K0	Rayleigh- Initial Stiffness Proportional Damping	1	5	2	5
DM6	KS	Rayleigh- Tangent Stiffness Proportional Damping (Secant Variation)	1	5	2	5
DM7	ZERO	Non Viscous Damping	1	0	2	0

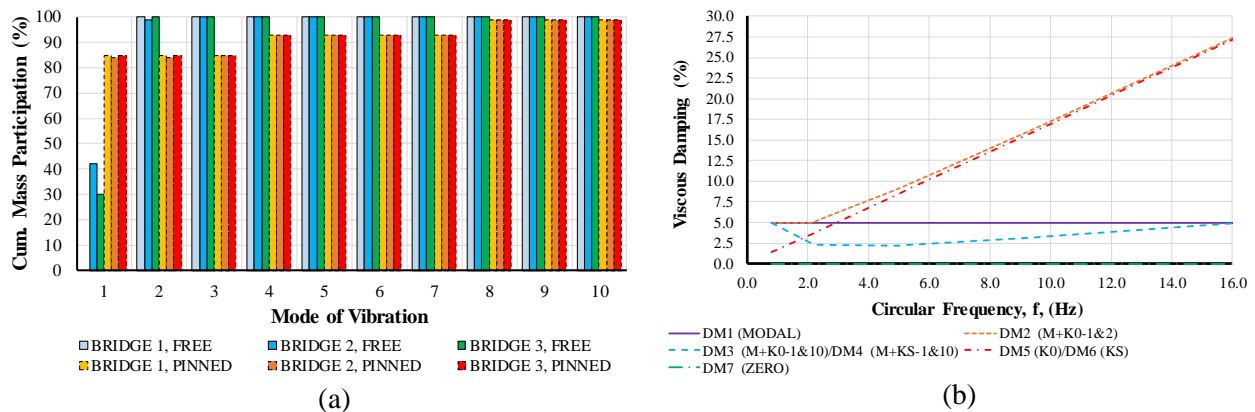


Fig. 4 – Distribution of Viscous Damping for Nonlinear Analysis; (a) Mass Participation in Transverse Direction for the three bridges with free and pinned abutments; (b) Viscous Damping per Damping Model for Bridge 1 with pinned abutments.

3.3 Nonlinear Analysis for Bridges with Pinned Abutments

The means of the maximum transverse displacements calculated using the seven pairs of ground motions spectrally matched to the design spectrum and for the seven damping models are shown in Figure 5. Figures 5(a), 5(b) and 5(c) correspond to the transverse nonlinear response for Bridges 1, 2 and 3, respectively.

Figure 5 shows that for bridges with pinned abutments there are three main behaviors. The first tendency is that the damping models Modal, M+K0-1&2, M+K0-1&10 and M+KS-1&10 have similar inelastic displacement patterns. All these responses are relatively close among them and this could be explained since these models are based on a classical Rayleigh damping approach. In these cases, the damping matrix is calculated using the mass and the stiffness proportional terms of Equation 1. For these scenarios, the mass proportional term (m) is dominating the inelastic response. Thus, regardless of what type of stiffness is used in the analysis (initial or tangent), the response will be similar for a Rayleigh damping model. These findings are in agreement with the results obtained by Priestley and Grant [4].

The second tendency corresponds to the behavior of the bridges with the stiffness proportional damping model (K0-1&2 and KS-1&2). In this situation, the KS-1&2 model has larger deformation demands than the K0-1&2 approach with differences varying between 3% and 6%. This is expected since the KS model is calculated



using the current stiffness of the structure instead of the initial elastic properties. Also, note that there is a displacement variation between the stiffness proportional model with tangent stiffness and the modal damping (lowest response) of 39%, 34%, and 44%, for the central columns of bridge 1, 2 and 3, respectively. The explanation of this behavior is not only that the stiffness proportional damping model is not using the mass term of Equation 1, but also the value of viscous damping ξ is lower than 5% for the first modes of the bridges.

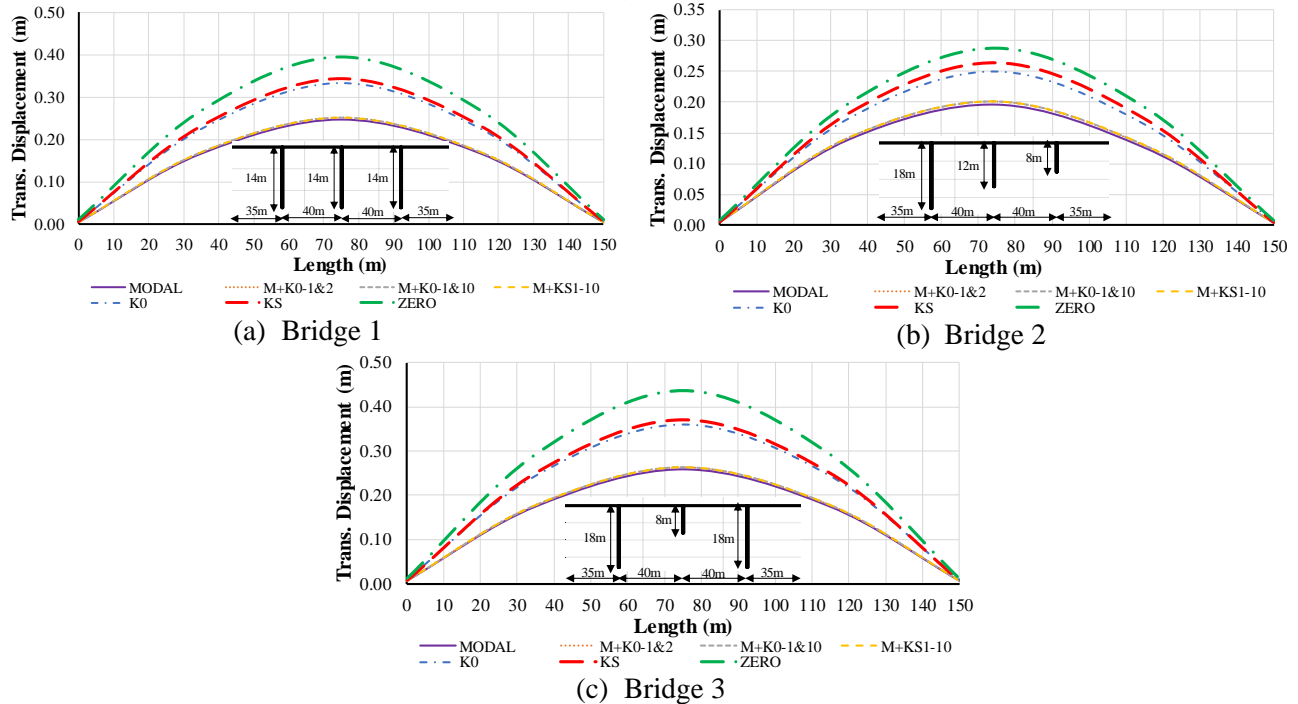
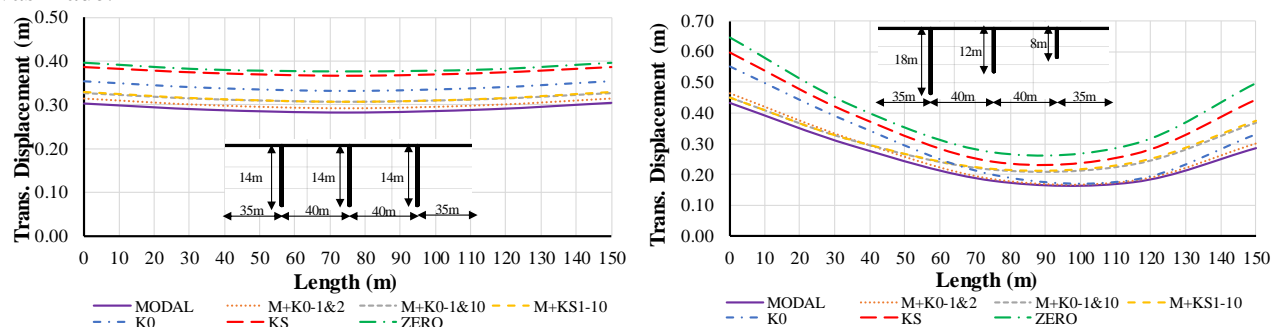


Fig. 5 – Transverse Displacement Profile with Pinned Abutments.

Lastly, the upper bound occurs when no viscous damping is deployed. As stated previously, some researchers [4] [7] believe that the non-viscous damping model is closer to the reality for nonlinear analysis of bridge structures because the amount of viscous damping that participates in the inelastic response is small. There are differences in the deformation demands between the lowest and highest responses for Bridges 1, 2 and 3, of 60%, 46%, and 69%, respectively. All these results demonstrate the high impact that the definition of the viscous damping model has on the deformation demands of bridges.

3.4 Nonlinear Analysis for bridges with Free Abutments

The same bridges were analyzed considering abutments that are free to translate. This is a more realistic scenario for bridges that are supported on elastomeric bearings and it is the normal assumption made by practitioners. Caltrans recommends in their design guide specifications [20] to model the abutments in the transverse direction with an elastic-plastic behavior having a yield displacement of 0.05m and a force of 30% of the vertical force on the abutments. For this case study, the conservative hypothesis of fully free translation was made.



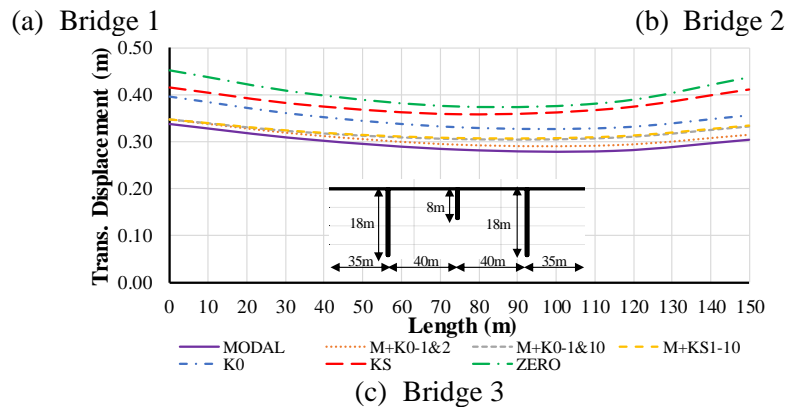


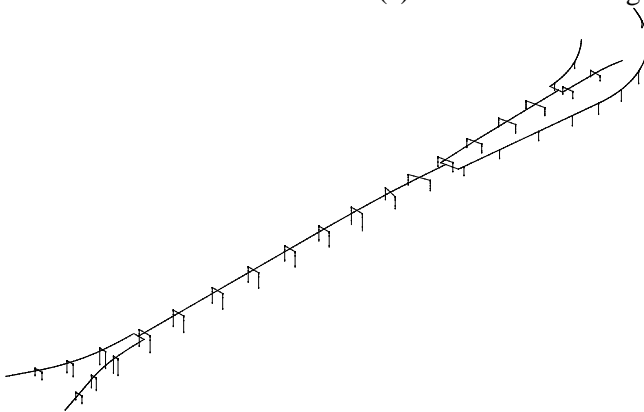
Fig. 6 – Transverse Displacement Profile with Free Abutments.

Figure 6 displays the transverse displacement profile for the three bridges with free abutments. For the three structures, the dispersion in the results is higher compared with the pinned abutment case. This is predictable since the inelastic behavior is concentrated in the columns, while with pinned abutments, the elastic damping of the superstructure participates in the seismic response. The Modal damping approach is always giving the lowest response. Also, notice how the Rayleigh damping models with mass and stiffness proportional terms are close among them, again showing that the mass term is dominating the inelastic response. A larger dispersion is seen for the stiffness proportional damping models with initial stiffness and tangent stiffness. In this case, a fairly constant difference of 10% for Bridge 1 is observed. For Bridge 2, there is a variation in the results from 8% to 46%, while Bridge 3 has differences between 6% and 13%. Comparing the extreme responses, a maximum difference in the results of 32%, 72%, and 76% is noted. These significant differences in the nonlinear results highlight the importance of a careful selection of a viscous damping model for structures that are modeled to translate freely in the transverse direction.

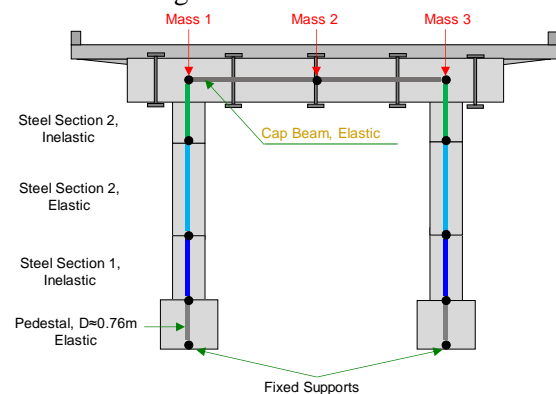
4. Anchorage Port Access Bridge



(a) Photo of Anchorage Port Access Bridge



(b) 3D Modeling of APA Bridge



(c) Lumped plasticity for two-column bent



Fig. 7 – Global Model of APA Bridge.

The last part of this paper shows the impact of viscous damping model assumptions on a real, irregular, large, and complex bridge: the Anchorage Port Access (APA) Bridge, a 787m long steel bridge. This structure was built in 1972 and currently is being assessed by the Alaska Department of Transportation (AKDOT) for seismic deficiencies. The main problem of the bridge is that its columns have slender and non-compact sections, allowing them to fail prematurely due to buckling and low displacement ductilities. Therefore, two half-scale tests of the piers 11 and 16 were constructed and tested at the Constructed Facilities Lab at NC State. The Piers 11 and 16 were selected because they have a D/t ratio of 80, and 44, respectively.

A 3D lumped plasticity spline model of the Anchorage Port Access Bridge was developed in Ruaumoko 3D to conduct nonlinear time history analyses. Figure 7(b) shows the model of the bridge. Some of the assumptions used in this model include: (1) the abutments are free to translate in both directions, (2) the columns are fixed at their base, and (3) the superstructure is continuous. In addition, Figure 7(c) exhibits the inputs used to conduct the nonlinear analysis. The plastic hinges are located at the ends of the columns, while the cap beams and the superstructure are modeled as elastic elements. This figure also displays the mass discretization. In this case, the recommendations given by Priestley et al. [16] were followed considering one-third of the column self-weight for the analysis.

4.1 Experimental Tests

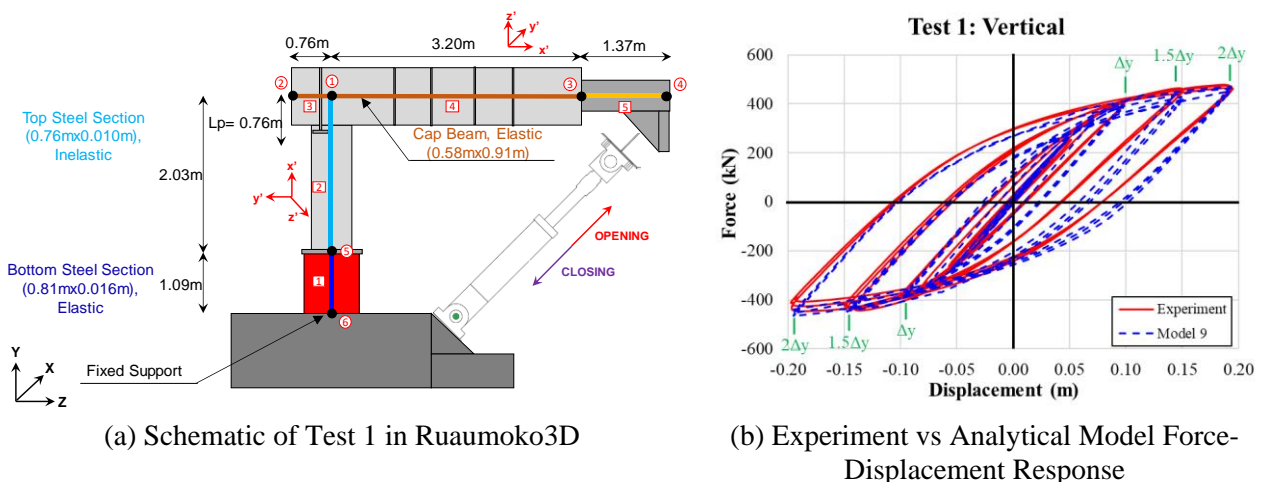
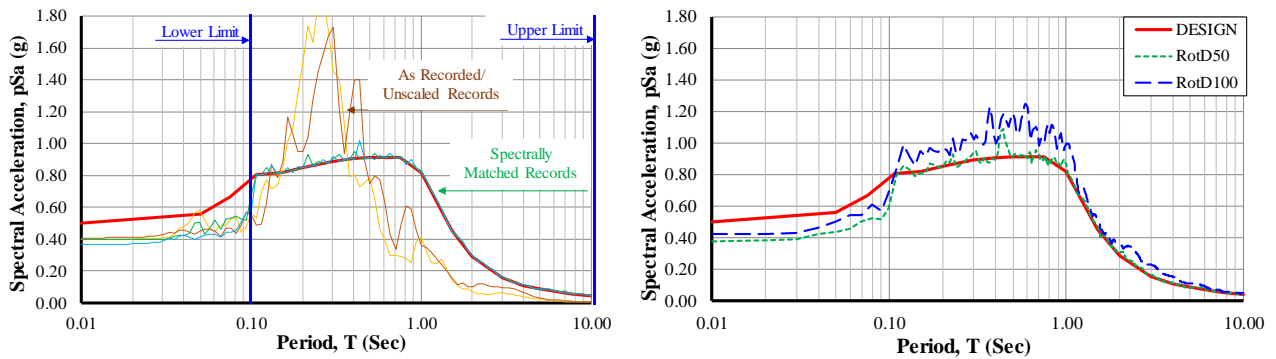


Fig. 8 – Model schematic and Force-Displacement response for Test 1.

The nonlinear analysis of the APA bridge was conducted using the hysteresis that best fit the experimental results. Figure 8(a) indicates the representation of Test 1 using a lumped plasticity approach in Ruaumoko 3D. In this case, the cap beam was modeled as an elastic element. In addition, Figure 8(b) exhibits a comparison of the vertical component of the force-displacement response given by the chosen hysteretic rule for the analysis (Ramberg Osgood with strength and cycle degradation) and the experiment. The hysteresis model effectively captures the linear and nonlinear behavior observed in the experiment up to a displacement ductility of 2.0. After that point, it is assumed that the column will buckle and will have rapid strength degradation.



4.2 Demands

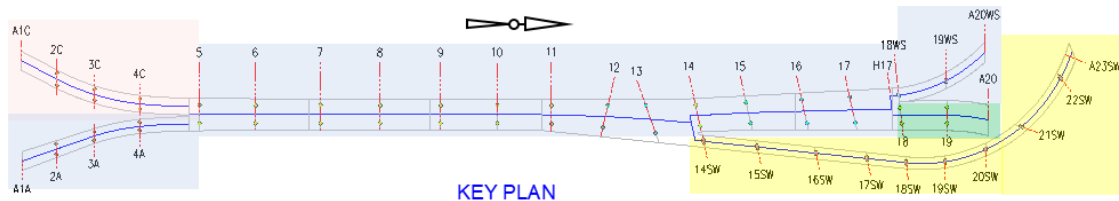


(a) As recorded ground motion spectrally matched to design spectrum

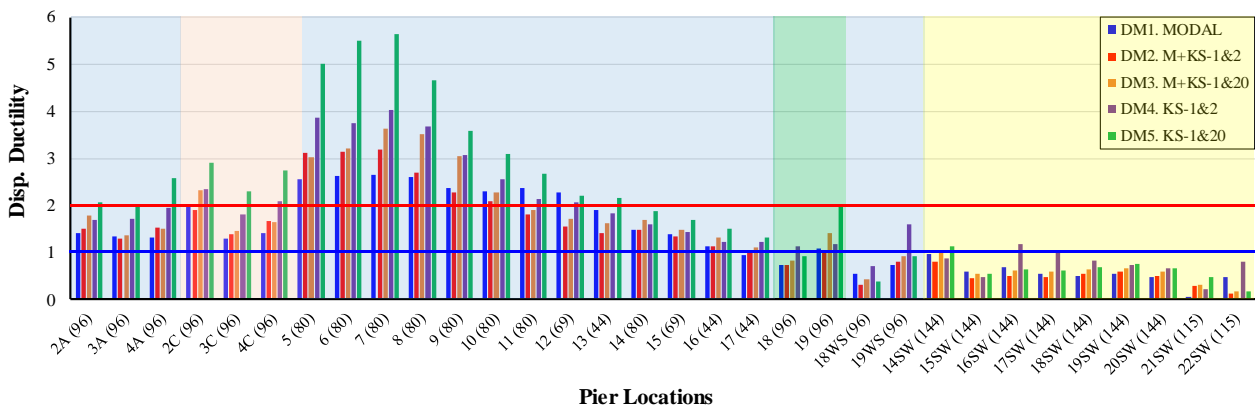
(b) RotD50 and RotD100 of spectrally matched records

Fig. 9 – Ground motion matching of as recorded motion of November 2018, Anchorage, AK earthquake.

The displacement demands on the bridge were calculated using the pair of ground motions recorded at the Port Access Station (NP8043) of the Anchorage earthquake that occurred on the 30th of November, 2018. The two components of the record were spectrally matched to a design spectrum, which was based on a previous Site-Specific Seismic Hazard Analysis study the AKDOT conducted [21]. The program ArtifQuakeLetII was used to perform the spectral matching of the records. Figure 9(a) shows the spectral match of the pair of ground motions for a range of periods from 0.1 to 10 seconds. On the other hand, Figure 9b) displays the calculation of the RotD50 and RotD100 of the spectrally matched records. In this circumstance, again, as in the case study of the three reinforced concrete bridges, the RotD50 of the ground motion matches the design spectrum well; thus, the two components of the matched earthquake do not need to be altered.



(a) Plan view of Port Access bridge



(b) Displacement ductility per each pier for the 5 damping models considered

Fig. 10 – Results in transverse direction of NLTHA for Anchorage record spectrally matched to design spectrum for a $F_y = 290$ MPa.

Figure 10 displays the nonlinear time history analysis for the bridge with the spectrally matched ground motions for five damping models and yield stress (F_y) of 290 MPa. These results were obtained by calculating



the envelope of maximum displacements for the pair of ground motions rotated each 15° . Five damping models were used to show the possible range of deformations at each pier. The following damping models were analyzed: Modal, Rayleigh (M+KS) and Stiffness Proportional Damping (KS) for two modes of vibration: 1&2 and 1&20 and 5% of viscous damping ratio because 90% of the mass participation in the transverse direction occurs before mode 20.

As shown in Figure 10(b), the maximum displacement demands on the bridge are concentrated between piers five and twelve. Moreover, it can be seen that there is a bigger dispersion in the results of the damping models in comparison with the three bridges analyzed in the previous section. This proves that the impact of viscous damping models on irregular structures is higher than for regular structures. In most of the piers that behave inelastically, the lowest response was associated with the Modal Damping. In addition, the data in the figure exhibits the importance of the selection of the second mode in the Rayleigh Damping for irregular structures, where the higher modes are essential. In this situation, there is a considerable variation in the results for Rayleigh damping with modes 1&2 and 1&20. It is seen that the higher modes of the DM2 model are overdamped. Furthermore, even for some piers such as 8 and 9, DM3 is very close to DM4 (stiffness proportional damping), which is the approach that gives the second largest response. This is only behind DM5, which is the damping model that used zero viscous damping. Finally, it is observed that in piers such as 6 and 7, there are differences higher than 100% between the extreme responses.

5. Conclusions

This study shows the profound impact that the selection of viscous damping has on the inelastic response of bridges. This was done by studying the nonlinear behavior of bridges in the transverse direction, considering three cases: (1) three RC bridges with pinned abutments, (2) three RC bridges with free abutments, and (3) the Anchorage Port Access Bridge. In all the cases, various damping models based on Rayleigh and Modal Damping were analyzed. For the RC bridges with pinned and free abutments, the mass term dominates the responses of Rayleigh Damping Models. Modal Damping is always lower than Rayleigh damping, but very similar in its responses. This can be explained because the higher modes had limited participation in the response of these bridges. Damping models based on stiffness proportional and zero viscous damping give the largest demands. In the case of the Port Access Bridge, the higher modes are important, producing considerable differences in the deformation demands of all the damping models considered in this paper. Finally, the numerical study conducted here highlights the importance of the selection of a proper damping model to obtain realistic deformation demands of bridges using NLTHA. Since there is not a consensus on what is the proper damping model that should be used in nonlinear analysis with lumped plasticity models, this topic is expected to be studied further.

6. Acknowledgements

The first author is pleased to acknowledge COLCIENCIAS and the Fulbright Association in Colombia for a scholarship to pursue his Ph.D. studies in the United States. Financial support from NC State University and the Alaska Department of Transportation and Public Facilities is also gratefully appreciated.

7. References

- [1] D. Chrisp, *Damping models for inelastic structures. Master's Thesis, University of Canterbury, Christchurch, New Zealand.* 1980.
- [2] Bernal Dionisio, "Viscous Damping in Inelastic Structural Response," *J. Struct. Eng.*, vol. 120, no. 4, pp. 1240–1254, 1994.



- [3] P. Léger and S. Dussault, "Seismic-Energy dissipation in MDOF Structures," *J. Struct. Eng.*, vol. 118, no. 5, pp. 1251–1269, 1992.
- [4] M. J. N. Priestley & D. N. Grant, "Viscous Damping in Seismic Design and Analysis," *J. Earthq. Eng.*, vol. 2469, no. September, pp. 229–255, 2005.
- [5] M. Kowalsky and U. Hasgul, "Impact of Viscous Damping Models on Nonlinear Response of SDOF Systems," *10th U.S. Natl. Conf. Earthq. Eng.*, 2014.
- [6] J. F. Hall, "Problems encountered from the use (or misuse) of Rayleigh damping," *Earthq. Eng. Struct. Dyn.*, vol. 35, no. 5, pp. 525–545, 2006.
- [7] F. a. Charney, "Unintended Consequences of Modeling Damping in Structures," *J. Struct. Eng.*, vol. 134, no. 4, pp. 581–592, 2008.
- [8] J. F. Hall, "Performance of viscous damping in inelastic seismic analysis of moment - frame buildings," *Earthq. Eng. Struct. Dyn.*, no. June, pp. 2756–2776, 2018.
- [9] A. K. Chopra and F. McKenna, "Modeling viscous damping in nonlinear response history analysis of buildings for earthquake excitation," *Earthq. Eng. Struct. Dyn.*, no. September 2015, pp. 193–211, 2016.
- [10] A. Carr, A. Puthanpurayil, O. Lavan, and R. Dhakal, "Damping models for inelastic time-history analyses - A proposed modelling approach," *16th World Conf. Earthq. Eng.*, vol. 1488, no. Abstract ID, p. 11, 2017.
- [11] A. J. Carr, *RUAUMOKO-3D - A program for inelastic time-history analysis. Department of Civil Engineering, University of Canterbury, New Zealand. 2004.*
- [12] L. Petrini, C. Maggi, M. J. N. Priestley, and G. M. Calvi, "Experimental verification of viscous damping modeling for inelastic time history analyzes," *J. Earthq. Eng.*, vol. 12, no. SUPPL. 1, pp. 125–145, 2008.
- [13] E. Smyrou, M. J. N. Priestley, and A. J. Carr, "Modelling of elastic damping in nonlinear time-history analyses of cantilever RC walls," *Bull. Earthq. Eng.*, vol. 9, no. 5, pp. 1559–1578, 2011.
- [14] Perform 3D User Guide, "Nonlinear Analysis and Performance Assessment for 3D Structures," *User Man. PERFORM 3D-Computer Struct.*, no. August, 2006.
- [15] C. Kong, "Rapid Direct Displacement-Based Assessment Approach for Bridge Structures," North Carolina State University, 2017.
- [16] M. J. N. Priestley, G. M. Calvi, and M. J. Kowalsky, *Displacement-Based Seismic Design of Structures. 2007.*
- [17] J. B. Mander, M. J. N. Priestley, and R. Park, "Theoretical Stress-Strain model for Confined Concrete," *J. Struct. Eng.*, vol. 114, no. 8, pp. 1804–1826, 1989.
- [18] D. M. Boore, "Orientation-independent, nongeometric-mean measures of seismic intensity from two horizontal components of motion," *Bull. Seismol. Soc. Am.*, vol. 100, no. 4, pp. 1830–1835, 2010.
- [19] L. A. Montejo and L. E. Suarez, "An improved CWT-based algorithm for the generation of spectrum-compatible records," *Int. J. Adv. Struct. Eng.*, vol. 5, no. 1, p. 1, 2013.
- [20] Caltrans, "Seismic Design Specifications- Second Edition State of California Department of Transportation May 2016," no. May, 2016.
- [21] URS, "Anchorage Port Access Bridge Site-Specific Seismic Hazard Analysis and Development of Seismic Design Ground Motions Report of Findings," 2013.